Received: 6 June 2017 | Revised: 22 July 2017 | Accepted: 23 July 2017

DOI: 10.1002/er.3851

RESEARCH ARTICLE

WILEY INTERNATIONAL JOURNAL OF ENERGY RESEARCH

Development of an ocean wave energy harvester with a built-in frequency conversion function

N.V. Viet[1] | Q. Wang[2] | A. Carpinteri[3]

[1] Department of Mechanics, Khalifa University, PO Box 127788, Abu Dhabi, UAE

[2] Department of Mechanics and Aerospace Engineering, Southern University of Science and Technology, Shenzhen 518055, China

[3] Department of Structural, Geotechnical, and Building Engineering, Politecnico di Torino, Corso Duca degli Abruzzi, Italy

Correspondence
N. V. Viet, Department of Mechanics, Khalifa University, PO Box 127788, Abu Dhabi, UAE.
Email: nguyen.viet@kustar.ac.ae

Summary

The research develops a novel harvester associated with a built-in frequency conversion device to harness energy from ocean waves based on the piezoelectric effect. The developed harvester consists of 2 generators driven by rotational motions converted from vertical motions by a rack and pinion actuator. The generator has a rotator with a magnetic bar attached to its blade tips and a stator. By this innovative design, the harvester is capable of converting ocean waves with low frequencies to mechanical vibrations with higher excitation frequencies of the piezoelectric transducer for increasing its energy conversion efficiency. A corresponding mathematical model for the harvester is developed to evaluate the generated power. The simulation results show that the generated power increases with increases in the ocean wave height, number of magnetic bars and decreases in the wave period, the distance between 2 opposite magnetic bars, and harvester's submerged part height. The power output is realized up to 260 W with the height, length, and width of the harvester being $1m \times 1m \times 1m$, at the ocean wave height and period being 2 m and 7 seconds, respectively.

KEYWORDS

frequency conversion, ocean waves, piezoelectric energy harvester, wave-structure interaction

1 | INTRODUCTION

Traditional fossil fuel sources such as oil, gas, and coal create pollution by releasing huge amount of carbon dioxide and other pollutants into the atmosphere. US Energy Information Administration indicates that the US electricity power sector has contributed more than one third of the total US energy-related carbon dioxide emissions in 2015.[1] The global warming at alarm level now is an inevitable result from the usage of such energy sources. Researchers are heading towards alternative abundant, renewable, and clean energy sources such as wind, solar, and ocean waves. Among these renewable energy sources, the ocean wave energy has a highest energy density, which is around 2 to 3 kW/m^2.[2-4] Besides, the strong and consistent energy demand on marine facilities, such as radar, communication devices, desalination devices, marine platforms, and electric charging station located on the offshore area is emerging.[5] Energy harvesting from ambient energy sources into usable electric power based on electrostatic, electromagnetic, and piezoelectric technology has been initiated and developed.[6] Remarkably, among these conversion technologies, the piezoelectric transducer possesses an energy density 3 times higher than the other 2 transducers.[7,8] The piezoelectric transducer has an effective conversion with no electric leakage when the excitation frequency of ambient vibration sources is higher than 10 Hz.[9] In addition, it was explored that the piezoelectric harvester's power output is

proportional to the cube of the excitation frequency.[7] Furthermore, in nature, the frequency of clean energy sources such as ocean waves, tidal, and wind is typically very low. Thus, piezoelectric energy harvesters with tuning devices for matching the frequencies are more efficient and effective than those without such tuning devices.[10] So far, the techniques for tuning the frequency of the ocean waves have a modest development. Murray and Rastegar[11] presented a 2-stage electrical energy generator based on the piezoelectric effect, which can convert the low-frequency ocean waves into much higher frequency mechanical vibrations. The simulation results indicated that the harvester efficiency is highly enhanced. Williams et al[7] proposed a dynamic model of a mass-spring-damper system that has an adjustable frequency device. Their theoretical analysis indicated that the amount of the increased power is proportional to the cube of the excitation frequency. The piezoelectric harvester magnifying the low excitation frequency of vibrational sources other than ocean waves to obtain a higher power was also intensively investigated.[7,12-16] Xie et al[16] presented a ring-shaped harvester using the magnetic effect and rotating velocity derived from wind flow and tidal current to increase the excitation frequency for a higher power output. The results showed that a power up to 5200 W could be realized for a practical design of the harvester with a radius around 0.5 m.

It is known that ocean waves own a source of powerful mechanical energy, but exhibit low frequencies. The energy conversion efficiency of the current renewable energy harvesting technologies, namely, electromagnetics, electrostatics, and piezoelectricity is low due to the mismatch of the frequencies of the waves and the harvesters. The aforementioned harvesters have been designed to convert the low-frequency wave into a higher frequency of mechanical vibration by using bending piezoelectric effect, which is 3 times lower than the tension/compression piezoelectric effect.[17] Hence, the produced power is still relatively low and only sufficient for small electric appliances.[11] One of the reasons is that the introduced technology able to tune the wave frequency by the bending piezoelectric effect is lower than other types such as tensional/compressional effect d_{33} and shear effect d_{15}. Current challenges remain to develop new piezoelectric energy harvesters from ocean waves with a higher electric generation efficiency. In addition, efficient and simple installations are also indispensable for a cost-effective design of the harvesters. In view of these challenges, the objective of the research is to propose a novel, simple, and efficient harvester using the tensional/compressional piezoelectric effect to convert a low-wave frequency into the higher frequency of mechanical vibration, which has not been fulfilled in literatures. In addition, the developed harvester includes a rack and pinion actuator to convert the vertical motion into the rotational motion. The generator has a rotator having a magnetic bar attached on its blade tips and a stator comprised of a mass, spring, lever, and piezoelectric transducer system (MLPS). By this novel design, the harvester is able to convert the low-frequency ocean waves into the higher excitation frequency of mechanical vibration, while the simple installation objective is also fulfilled.

2 | DESIGN AND MODELING OF HARVESTERS

2.1 | Analysis of the ocean wave-structure interaction

This section focuses on the derivation of the mathematical heaving modeling for harvesters having a cube shape subjected to ocean waves based on information in published literatures[18,19] in the ocean wave engineering. Wherein, factors appearing in the interaction are fully presented and included in the equations. Generally, the ocean waves can be classified as 3 categories: linear wave sinusoidal profiles, nonlinear waves described by nonsymmetrical profiles, and random seas predictable in the frequency domain. These waves are created by several phenomena, eg, winds, moving bodies (ship, boat...), seismic activities (earthquakes), motions of moon, and sun. The wave-structure interaction in 3D space is sketched in Figure 1. The still water level is defined as the average water surface elevation at any moment. Notations, h and $\eta(t,x)$ are water depth and vertical free surface displacement, respectively, both measured from the still water level. L_w, H_w, and c are wave length, wave height, and phase velocity of waves, respectively. d_m is the height of the submerged part of the harvester box, which is defined as a distance between the harvester bottom and the still water level. It is noted that d_m can be adjusted by changing the harvester ballast material, and still water level is not always coincident with the horizontal center plane of the harvester body.[18] Under the impact of ocean waves in x-y-z coordinates, a rigid floating body has 6 components of motions corresponding to 6 degrees of freedom. These components can be visualized in Figure 1 and commonly defined in ocean wave mechanics to be as follows: surge: displacement along x axis; sway: displacement along y axis; heave: displacement along z axis; roll: rotation about x axis; pitch: rotation about y axis; and yaw: rotation about z axis.

In this research, the linear ocean waves are considered based on literature.[18] It has been known that the

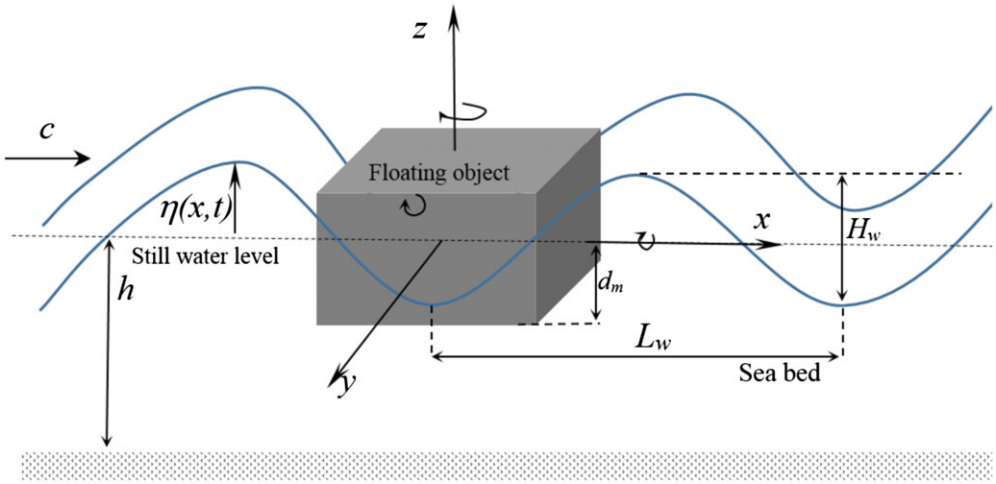

FIGURE 1 Floating cubic structure on the ocean floor in 3D space [Colour figure can be viewed at wileyonlinelibrary.com]

wavelength is a function of water depth, h, wave period, T and gravitical acceleration, $g = 9.8$ m/s^2, and can be computed by the iterative solution of the equation shown below[18]

$$L_w = \frac{gT^2}{2\pi} tanh\left(\frac{2\pi h}{L_w}\right), \tag{1}$$

From Equation 1, the wavelength is only dependent on the wave period and water depth.

Consequently, the corresponding wave number, k, wave celerity, c, and the wave frequency, ω can be provided as:

$$k = \frac{2\pi}{L_w} \; ; c = \frac{L_w}{T} \text{ and } \omega = kc = \frac{2\pi}{T}, \tag{2}$$

The wave power by a harvester for a deep-water condition in the direction of the wave propagation can be expressed as[18]

$$P_w = \frac{\rho g^2 H_w^2 T W_o}{32\pi}, \tag{3}$$

where W_o is also equal to the wave crest width.

Analysis of the interaction between ocean waves and a symmetric floating body is difficult in 3-dimensional (3D) space, as the motions in 6 degrees of freedom can be simultaneously appeared and arbitrarily interchanged between the 2 motions. The purpose of an effective harvester design is to optimally facilitate and adopt only the heaving motion; thus, pure motions such as surge and pitching in x-z coordinate system shall be removed. To do so, the floating structure is fixed in directions other than z-direction as shown in Figure 2; by this way, pitching and surging motion are removed.[18] As harvester vibrates only in the z-direction, the harvester keeps heaving irrelevant of the ocean wave length. After these considerations, the heaving motion of the harvester under the impact of ocean waves is analyzed and established by ocean wave mechanics and, subsequently, employed to calculate the harvester's electric power output.

To establish the motion of the harvester, Newton's second law is used. The equation of the heaving motion of a floating rigid body, ie, the harvester, can be fully expressed by the following equation [18]

$$\begin{aligned} M_s\frac{d^2z}{dt^2} + M_a\frac{d^2z}{dt^2} + D_v\left(\frac{dz}{dt}\right)\left|\frac{dz}{dt}\right|^N + D_r\frac{dz}{dt} + D_p\frac{dz}{dt} \\ + \rho g L_o W_o z + N q_s z = F_{z0}\cos\left(\omega t + \gamma_z\right), \end{aligned} \tag{4}$$

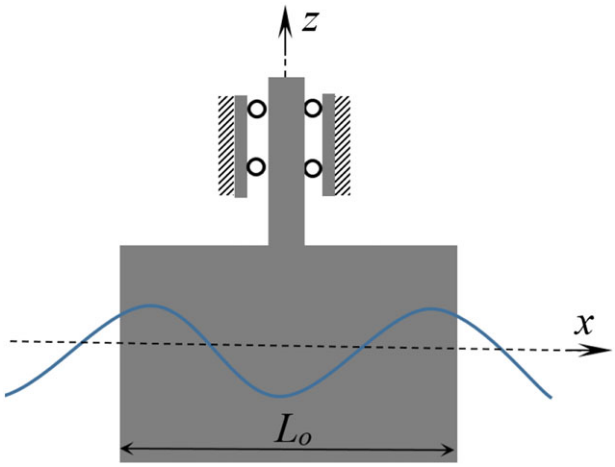

FIGURE 2 2D wave-structure interaction [Colour figure can be viewed at wileyonlinelibrary.com]

where M_s is mass of the submerged part of the harvester that is equal to mass of displaced water and can be computed as

$$M_s = \rho d_m L_o W_o, \tag{5}$$

M_a in Equation 4 is the added mass that is the inertia applied to the harvester due to the presence of its body in a moving fluid or due to the motion of its body in a stationary fluid.[18] The added mass is dependent on the frequency of ocean waves.[20-22] Because this work is to develop a harvester working in less varying frequencies, the simplified form of the added mass introduced in literature[19] is used as

$$M_a = \frac{\varphi_m \pi \rho L_o {W_o}^2}{4}, \tag{6}$$

where φ_m is the added-mass coefficient, which can be computed for a rectangular body[23] as

$$\varphi_m = 0.437e^{-0.8813W_o/d_m} + 0.6854e^{-0.009974W_o/d_m}, \tag{7}$$

D_v and D_r in Equation 4 are the viscous and radiation damping coefficients, respectively. These are results of the energy loss due to waves created by harvester motion on the water surface. For the rectangular structure in Figure 1, the viscous damping coefficient is approximated to be[18]

$$D_v \simeq \frac{\rho C_d L_o W_o}{2}, \tag{8}$$

where C_d is drag coefficient, and it is equal to 1.05 for a rectangular body.[24] The radiation damping coefficient is given by[18]

$$D_r = \frac{\rho L_o g^2}{\omega^3} R_Z^2, \tag{9}$$

where R_z is the ratio of the radiated-wave amplitude to the body motion amplitude, which is defined as

$$R_z = 2e^{-\frac{\omega^2}{g}d_m} \sin\left(\frac{\omega^2 W_o}{2g}\right), \tag{10}$$

$D_p$in Equation 4 is the power takeoff coefficient, which is an amount of the ocean wave energy converted into the electric energy by a harvester and the energy loss by the internal structure friction.[18] In this work, only the harvester-generated electric energy loss and the internal structure energy loss, eg, viscous damping and internal structure friction of lever, are considered as the power takeoff. Other energy losses such as the fiction between the gear and gear rack are ignored in this study. By defining D_t as a power takeoff coefficient of 1 generator, we have a relationship of $D_p = 2D_t$ because there are 2 generators in 1 harvester. The mathematical formulation of the coefficient D_t will be discussed profoundly the in next section. Notations ρ and q_s in Equation 4 are the density of seawater (1030 kg/m^3) and the spring constant of mooring lines; and N is the number of lines (mooring restoring force). The harvester is designed to be freely heaved upward and downward without any restriction from mooring line; hence, the spring constant and mooring line number are considered to be $N = q_s = 0$.

F_{z0} in Equation 4 is the amplitude of the wave-induced heaving force, which is computed as[19]

$$F_{z0} = \frac{\rho g H_w W_o L_w}{2\pi}\left(e^{-\frac{2\pi d_m}{L_w}} + 1\right) sin\left(\frac{\pi L_o}{L_w}\right), \tag{11}$$

γ_z in Equation 4 is the phase angle between the wave and the force. Because the harvester is designed to be symmetric about planes x-y and y-z, γ_z is set to be zero.[19]

By taking into account of the given values of $N = q_s = \gamma_z = 0$ and employing the steady solution, the solution form of Equation 4 is characterized as

$$z = z_0 \cos(\omega t + \gamma_z - \theta_z), \tag{12}$$

where z_0 is the amplitude of the harvester heave motion and θ_z is the phase angle between the wave force and motion direction. The amplitude is thus obtained to be[18]

$$z_0 = \frac{\frac{F_{z0}}{(\rho g W_o L_o)}}{\left[\left(1 - \frac{\omega^2}{\left(\frac{\rho g W_o L_o}{M_s + M_a}\right)}\right)^2 + \left[\frac{\omega\left(D_r + D_v + D_p\right)}{\rho g W_o L_o}\right]^2\right]^{1/2}}, \tag{13}$$

and

$$\theta_z = tan^{-1}\left[\frac{\frac{\omega\left(D_r + D_v + D_p\right)}{\rho g W_o L_o}}{\left(1 - \frac{\omega^2}{\frac{\rho g W_o L_o}{M_s + M_a}}\right)}\right], \tag{14}$$

It can be seen from Equations 9 to 14 that the amplitude, damping coefficients, and angles are dependent on the ocean wave frequency. By substituting Equations 13

and 14 into Equation 12, we obtain a full heave motion equation of the harvester as follows:

$$z = \frac{\frac{F_{z0}}{(\rho g W_o L_o)}}{\left[\left(1-\frac{\omega^2}{\frac{\rho g W_o L_o}{M_s+M_a}}\right)^2 + \left[\frac{\omega\left(D_r+D_v+D_p\right)}{\rho g W_o L_o}\right]^2\right]^{1/2}} \cos\left\{\omega t - tan^{-1}\left[\frac{\frac{\omega\left(D_r+D_v+D_p\right)}{\rho g W_o L_o}}{\left(1-\frac{\omega^2}{\frac{\rho g W_o L_o}{M_s+M_a}}\right)}\right]\right\}, \quad (15)$$

The ocean data used in this work are provided in Table 1, unless otherwise noted.

2.2 | Root mean square of the generated power

2.2.1 | Magnetic force

The harvester with 2 internal generators freely heaves in z-direction under the interaction from the ocean waves as shown in Figure 3A. Each generator has a cubic shape with an edge length of $D = 0.8$ m. It can be seen from Figure 3C that each generator has a rotator and a stator. The rotator consists of m rotator blades with a length of r. Each tip of blades is attached with a magnetic bar. The stator contains an MLPS. The distance between 2 opposite magnetic bars is set as d. When the harvester heaves, the gear rack moves upward and downward accordingly and then drives the generator rotator to rotate via the gear and shaft devices. As the rotator rotates, the distance between 2 magnetic bars, d, varies leading to a change of magnitude of repelling magnetic force, F_r.[16] As a result, the MLPS is excited by the magnetic force.

The angular frequency of the repelling force, F_r, between 2 magnetic bars (between rotator and stator tips) is linearly dependent on the reciprocal angular speed of the rotator. Therefore, the frequency of the magnetic force can be increased by adjusting both the rotator speed and rotator blade number to achieve a higher power output. In addition, a higher force frequency could avoid a possible electric leakage of the harvester.[9] As shown in Figure 3B, the gear rack is fixed to the harvester basement; thus, the reciprocally vertical speed of the gear rack is equal to the harvester speed. In this research, because the repelling magnetic force is used as a sinusoidal function of the vertical speed of gear rack, the average speed value is used instead of instantaneous one. From Equation 15, the average vertical speed of the gear rack, $\lambda_{a.rz}$, can be written as

$$\lambda_{a.rz} = \frac{4z_0}{T} = \frac{\frac{4F_{z0}}{(T\rho g W_o L_o)}}{\left[\left(1-\frac{\omega^2}{\frac{\rho g W_o L_o}{M_s+M_a}}\right)^2 + \left[\frac{\omega\left(D_r+D_v+D_p\right)}{\rho g W_o L_o}\right]^2\right]^{1/2}}, \quad (16)$$

The correspondingly average angular speed of rotor, ω_r, can now be calculated to be

$$\omega_r = \frac{\lambda_{a.rz}}{r} = \frac{\frac{4F_{z0}}{(rT\ \rho g W_o L_o)}}{\left[\left(1-\frac{\omega^2}{\frac{\rho g W_o L_o}{M_s+M_a}}\right)^2 + \left[\frac{\omega\left(D_r+D_v+D_p\right)}{\rho g W_o L_o}\right]^2\right]^{1/2}}, \quad (17)$$

where r is the rotator radius as shown in Figure 3C.

Because the repelling magnetic force is a function of the gap, d, and time, t, the repelling magnetic force in 1 generator is considered as absolute sinusoidal form as shown below[16]

$$F_r(t) = |F_{r0}\sin(m.\omega_r.t/2)|, \quad (18)$$

where m and F_{r0} are rotator blade number and the amplitude of repelling magnetic force, respectively. From available experimental results,[25] when the minimal distance between 2 opposite magnetic bars on the rotator and stator is set as d, the repelling force amplitude F_{r0} between 2 magnetic bars can be calculated by:

$$F_{r0} = c_2 c_1^{4/3}\Theta_r|\Theta(d)|\Psi(d), \quad (19)$$

where, c_1, c_2, and c_3 are height, length, and width of the magnetic bar, respectively as shown in Figure 3C. The magnetic bar is selected as Neodymium iron boron, N5311,[26] having a known equivalent magnetic residual flux density denoted as $\Theta_r = 1.45$ T. The material properties and dimensions of the components are provided in Table 2, unless otherwise noted. $\Theta(d)$ and $\Psi(d)$ are defined as the magnetic flux density field and the decay function of repelling force between 2 magnetic faces, respectively. For a rectangular magnet, functions $\Theta(d)$ and $\Psi(d)$ can be obtained as[27]

$$\Theta(\mathrm{d}) = \frac{\Theta_r}{\pi}\left[tan^{-1}\left(c_1c_2/\left\{2d\sqrt{4d^2+{c_1}^2+{c_2}^2}\right\}\right) - tan^{-1}\left(c_1c_2/\left\{2(c_1+d)\sqrt{4(c_1+d)^2+{c_1}^2+{c_2}^2}\right\}\right)\right], \quad (20)$$

TABLE 1 Ocean wave properties

T, s	h, m	c_d	H_w, m	d_m, m
7–15	30	1.08	1–5.5	0.1–0.5

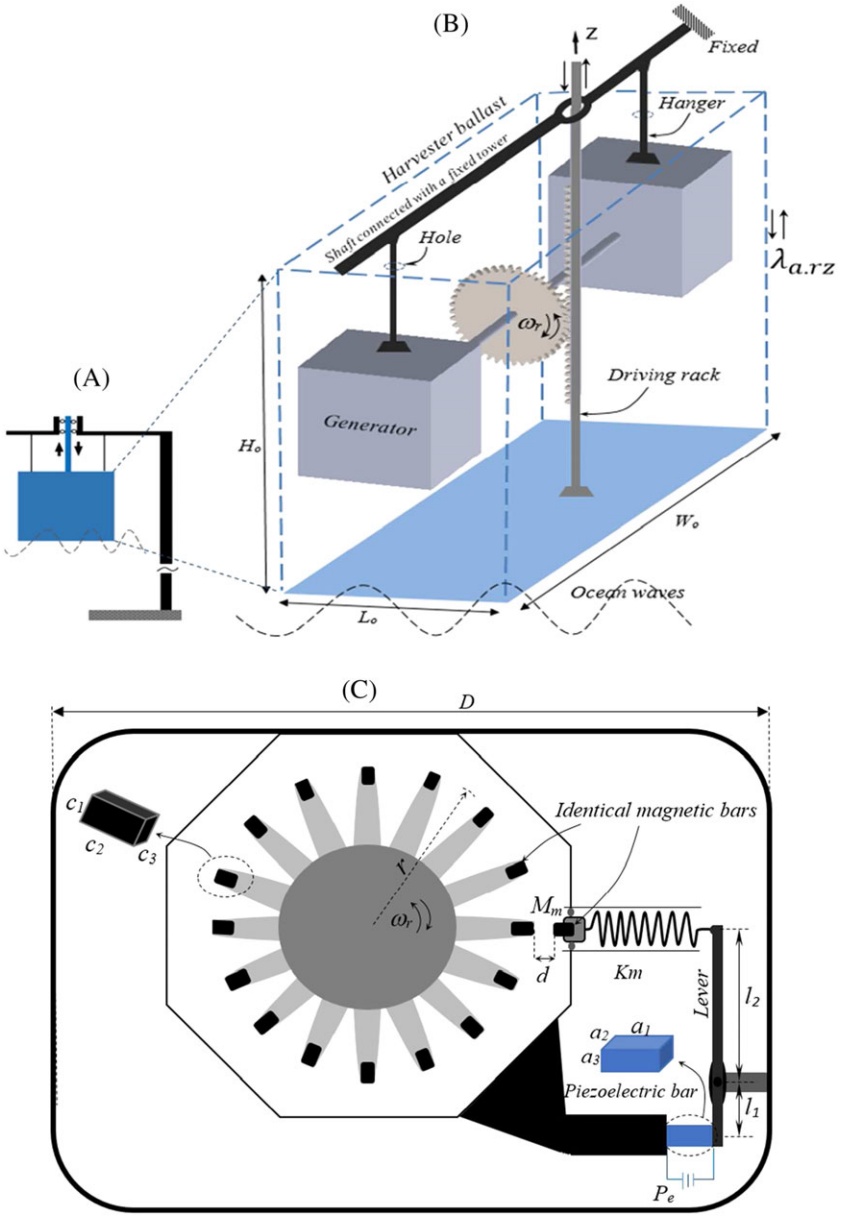

FIGURE 3 Structural design of harvester. A, Interaction of harvester and ocean waves, B, harvester's internal structure, and C, generator's internal structure [Colour figure can be viewed at wileyonlinelibrary.com]

and

$$\psi(d) = \left(1.749 + 1.144e^{\left(-\frac{d}{d_0}\right)}\right) \times 10^6 \left(\mathrm{NT^{-2}m^{-7/3}}\right), \quad (21)$$

where d_0 is standardly selected as 1 mm.

2.2.2 | Root mean square of the generated power

The MLPS consists of a mass-spring system and a lever fixed with a piezoelectric bar as shown in Figure 4A. The repelling magnetic force drives the MLPS to generate the usable electric power. In order to evaluate the power output, the MLPS can be converted into a 2-degrees-of-freedom model[28] and shown in Figure 4B. Based on Figure 4A, the MLPS has a vibrational mass, m_m, and a connecting spring with spring stiffness, K_m. The vibrational mass is attached with small rolling wheels to reduce the friction between the moving mass and generator's frame at a fullest extent. The vibrational mass is a combination of housing mass, M_h, and magnetic bar mass, M_g, and therefore the relation $M_m = M_h + M_g$ is set. In Figure 4A, the lever made of steel having a long moment arm, l_2, and short moment arm, l_1, is able to freely rotate around point, B, and its equivalent lever moment ratio is defined as $n_l = l_2/l_1$. Value $l_1 = 0.02$ m is chosen throughout the research. Both tips of the lever are firmly fixed with the mass-spring system and piezoelectric transducer at points C and A, respectively, as shown in Figure 4A.

TABLE 2 Harvester material properties and dimensions

Rotator's component dimensions	MLPS's component dimensions	Mass	Stiffness
$c_1 = c_3 = 0.025$ m	$n_l = 10–15$	$M_m = 0.5$ kg	$K_m = 20$ kN/m
$c_2 = 0.05$ m	$\xi = 0.0017$	--	--
$m = 4–18$	$a_2 = a_3 = 0.015$ m	--	--
$r = 0.25$ m	$a_1 = 0.1$ m	--	--
$d = 0.0015–0.0024$ m	$l_1 = 0.002$ m	--	--
$C_v = 0.375$ (nF) for piezoelectric patch with geometry of 0.01 m, 0.01 m, and 0.0001 m.			

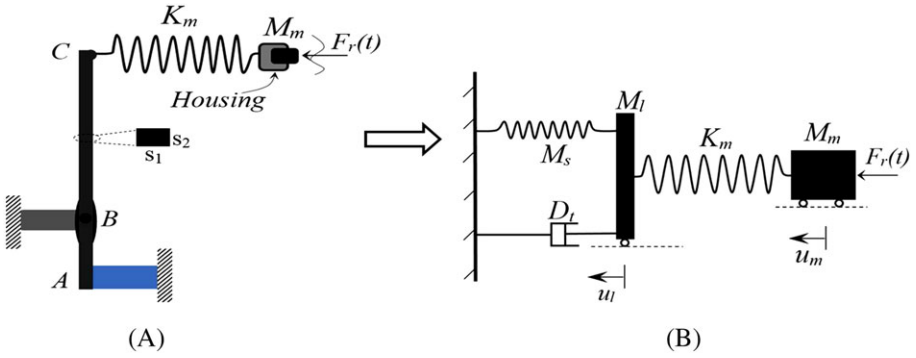

FIGURE 4 Model conversion of MLPS into a 2-degrees-of-freedom system. A, MLPS and B, 2-degrees-of-freedom system [Colour figure can be viewed at wileyonlinelibrary.com]

The piezoelectric bar with a length of a_1, a width of a_2, and a height of a_3 is made of the lead zirconate titanate (PZT4). The parameters of the mass-spring-damper system can be derived from material properties and dimensions of the equivalent cantilever beam[29]

$$K_l = E_l.s_1^3 s_2/\left(4.l_1^3.n_1^3\right), \quad M_l = \rho_l.A_l.l_l.n_l \quad , \text{ and } D_l = 2.\xi.\sqrt{K_l.M_l}, \tag{22}$$

where E_l, ρ_l, A_l, D_l, and ξ are Young's modulus, material density, cross-section area, mechanical damping coefficient, and damping ratio of lever arms, respectively. Notation K_l is the spring constant corresponding to the elastic deflection of beam tip, C; D_l is the coefficient of mechanical damping force of the beam, that is induced by the internal structural damping force[30] and the friction between the cantilever beam and the viscous air in vibration process. Besides the elastic deflection of the lever, the axial deformation of the piezoelectric bar also has a small contribution to the spring constant modeled by, $K_p = E_p.a_2^2/(a_1.n_l^2)$. The equivalent spring constant, K_s, of the lever-piezoelectricity device now can be obtained as $K_s = K_l.K_p/(K_l + K_p)$. The face of the lever arm is designed as a rectangular shape with a height and width of s_1 and s_2, respectively, as shown in Figure 4A.The dimensions of the lever face are selected as $s_1 = 0.03$ m and $s_2 = 0.015$ m, unless otherwise noted. The total damping coefficient, D_t, of the MLPS consists a damping coefficient, D_l, of lever and electric damping coefficient, D_e , from a closed electric circuit,[31] which links directly to piezoelectric transducer. Thus, the harvester damping coefficient may be written as $D_t = D_e + D_l$, where the electrical damping coefficient, D_e, can be derived as[32]:

$$D_e = n^2 d_{33}^2 K_s^2/\left(\pi^2 c_a.f_n\right), \tag{23}$$

In Equation 23, d_{33} is the tension/compression piezoelectric effect in the polling direction, which is firmly selected as $d_{33} = 3.10^{-10}$ (C/N); c_a is the electric capacity of the piezoelectric bar; and f_n is the first natural vibration frequency of the spring-mass system as shown in Figure 4 B. The first natural vibration frequency of the system can be determined by using the numerical solution.[33]

Once the components of the MLPS model are introduced, the force applied to the piezoelectric transducer and the generated output power of harvester can be derived hereafter. According to Newton's second law, the governing equation of the MLPS depicted in Figure 4B can be characterized as follows:

$$\begin{cases} \ddot{u}_m = \dfrac{K_m(u_l - u_m)}{M_m} + \dfrac{F_r(t)}{M_m} \\ \ddot{u}_l = \dfrac{K_m(u_m - u_l)}{M_l} - \dfrac{K_s u_l}{M_l} - \dfrac{D_t \dot{u}_l}{M_l} \end{cases} \tag{24}$$

The iteration method is used to solve Equation 24. Namely, the state-space method is firstly used to reduce the second-order-differential equation system to a first-order-differential equation system:

$$\begin{cases} \dot{u}_m = \lambda_m \\ \dot{u}_l = \lambda_l \end{cases} \Rightarrow \begin{cases} \dot{\lambda}_m = \ddot{u}_m \\ \dot{\lambda}_l = \ddot{u}_l \end{cases}, \tag{25}$$

where λ_m and λ_l are the velocities of the vibrational mass and tip, B of the lever, respectively. Subsequently, from Equations 24 and 25, a system of the first-order differential equations is written as functions

$$\begin{cases} \dot{\lambda}_m = f_1(t, u_m, u_l) \\ \dot{\lambda}_l = f_2(u_m, u_l, \lambda_l), \\ \dot{u}_m = f_3(\lambda_m) \\ \dot{u}_l = f_4(\lambda_l) \end{cases} \tag{26}$$

The time step Δt in the numerical solution is selected as 10^{-4} seconds. As a result, the displacements and velocities of the vibrational mass and lever at the time t_{i+1} can be derived as:

$$\begin{cases} t_{i+1} = t_i + \Delta t \\ \lambda_m(t_{i+1}) = \lambda_m(t_i) + f_1(t_i, u_m(t_i), u_l(t_i)).\Delta t \\ \lambda_l(t_{i+1}) = \lambda_l(t_i) + f_2(u_m(t_i), u_l(t_i), \lambda_l(t_{i+1})).\Delta t, \quad i = 0, 1, 2...\infty. \\ u_m(t_{i+1}) = u_m(t_i) + f_3(\lambda_m(t_{i+1})).\Delta t \\ u_l(t_{i+1}) = u_l(t_i) + f_4(\lambda_l(t_{i+1})).\Delta t \end{cases} \tag{27}$$

The initial conditions of the MLPS are set to be zero values, ie, the expressions of initial displacements and vibrational velocities are shown: $i = 0$, $t_0 = 0$, $u_m(t_0) = 0$, $u_l(t_0) = 0$, $\lambda_m(t_0) = 0$, and $\lambda_l(t_0) = 0$. Subsequently, the force $F_A(t)$ at lever tip A applied to the piezoelectric bar can be computed to be:

$$F_A(t_i) = n_l.F_l(t_i) = n_l.K_s.u_l(t_i), \tag{28}$$

Then, the electric charge, voltage, and current generated by the piezoelectric effect at time t_i are expressed as:

$$\begin{cases} Q(t_i) = d_{33}.n_l.K_s.u_l(t_i) \\ V(t_i) = d_{33}.n_l.K_s.u_l(t_i)/c_a \\ I(t_i) = d_{33}.n_l.K_s.\lambda_l(t_i) \end{cases}, \tag{29}$$

where d_{33} is compression piezoelectric effect. The electric capacity of the piezoelectric material can be computed as[34]

$$c_a = c_v x a_2 x a_3 x 0.0001/(0.01 x 0.01 x a_1), \tag{30}$$

The value of c_v is provided in Table 2. The electric power output of 1 generator at time t_i from the piezoelectric effect now can be described as:

$$P_{e1}(t_i) = d_{33}^2.n_l^2.K_s^2.u_l(t_i).\lambda_l(t_i)/c_a, \tag{31}$$

When the harvester works for a time duration T_d, RMS of the generated electric power from time 0 to T_d can be computed by:

$$P_{e1}^{rms} = \sqrt{\frac{1}{T_d}\int_0^{T_d} P_{e1}^2(t).dt}, \tag{32}$$

When T_d is divided into σ small time intervals, the discrete expression of Equation 32 can be rewritten as:

$$P_{s1}{}^{rms} = \sqrt{\frac{1}{\sigma}\sum_{i=1}^{\sigma} P_{e1}^2(t_i)}, \tag{33}$$

The conversion efficiency of harvester now can be written as

$$f_e = \frac{2.P_{s1}^{rms}}{P_w} 100\%, \tag{34}$$

3 | RESULTS AND DISCUSSIONS

The effectiveness of the harvester system is evaluated by examining the effects of the ocean wave properties and the harvester component's material properties and dimension using the developed mathematical model. A comparison between the proposed harvester and snake-like structure Pelamis in terms of power output is also implemented to show the efficiency of the developed harvester. The ocean wave properties and the internal component's material properties and dimensions of the harvester in the simulations are provided in Tables 1 and 2, respectively, unless otherwise noted.

To understand the soundness of the developed harvester and its modeling, the reciprocal heave motion of the harvester and relative displacement of the vibrational mass are shown in Figure 5A,B, respectively. The data used in this simulation are provided in Tables 1 and 2 and other parameters are selected as $n_l = 15$, $m = 15$, $d = 0.002$ m, $T = 7$ seconds, $Wo = 1$ m, $H_w = 1.5$ m, and $d_m = 0.25$ m. It is observed from Figure 5A that the harvester oscillates with a period equal to that of ocean waves being $T = 7$ seconds, but with a different amplitude as $z_0 = 0.7$ m, which is 0.05 m smaller than ocean wave amplitude, $H_w/2$. It is also observed from the figure that the vibrational mass vibrates with a frequency of 4 Hz, which is 30 times higher than that of the ocean waves (0.13 Hz). Hence, it is concluded that by using and

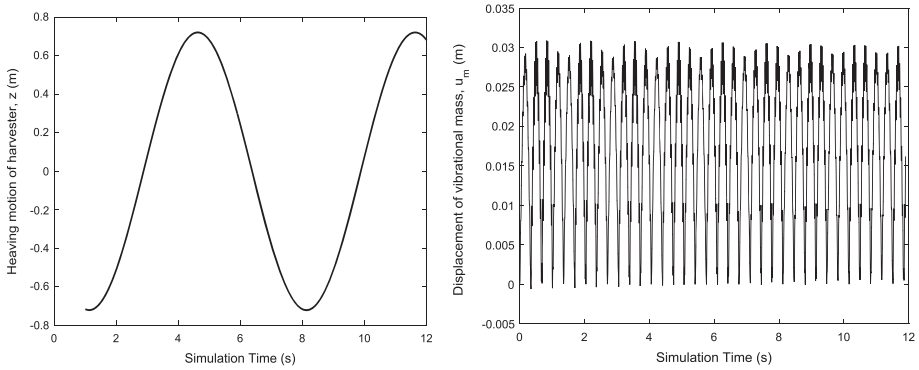

FIGURE 5 Vibrational displacement: A, heaving motion of harvester and B, vibrational mass

increasing the relative movement between the rotator magnetic bar and magnetic bar embedded on the vibrational mass, the low-frequency ocean waves are converted into a higher mechanical frequency of the MLPS.

The effect of properties and dimensions of ocean waves and harvester's components on the RMS of the generated electric power is investigated. Figure 6 shows the effect of the height of the submerged part of the harvester on the RMS of the power output at various wave heights of $H_w = 1$ m, 1.5 m, and 2 m. Other parameters are selected as $n_l = 15$, $m = 15$, $d = 0.002$ m, $T = 7$ seconds, and $Wo = 1$ m. It is shown in Figure 6 that the RMS decreases nonlinearly with an increase in the submerged height. Specifically, when the submerged height, d_m, varies from 0.1 m to 0.5 m, the RMS decreases from 273 W to 245 W with a wave height of 2 m. The RMS of 1 generator can reach up to 260 W at a submerged part height and a wave height of $d_m = 0.3$ m and $H_w = 2$ m, respectively. It is known that the height of the submerged part of the harvester can be manually adjusted by changing the material of harvester ballast.[18] The simulation

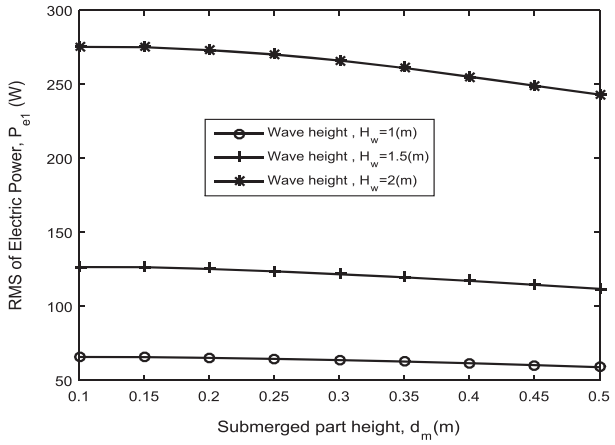

FIGURE 6 Effect of the submerged height of harvester on RMS of the power with different wave height

result is interpreted by the fact that an increase in the submerged height can lead to a rise in wave viscous and radiation damping, which are characterized in Equations 8 and 9. In addition, it is also observed in the figure that a rise in wave height leads to an increase in the power output. It can be explained that, from Equations 11 and 17, the average angular frequency of the reciprocally repelling magnetic force, ω_r, is linearly propositional to the wave height. Thus, increasing the wave height results in a corresponding rise in angular frequency of magnetic force leading to a higher electric power output.

Figure 7 depicts the variation of RMS with respect to the wave height at $n_l = 15$, $m = 15$, $d = 0.002$ m, $T = 7$ seconds, $d_m = 0.25$ m, and $Wo = 1$ m. It indicates a nonlinear increment of power output with respect to the rise in wave height. That is, an increment of the wave height from 2 m to 5.5 m leads to the rise in the power output generated by 1 generator from 273 W to 1500 W. The observation is interpreted on one hand that based on Equations 8 and 9, there is no increment of damping force with the increment of wave height. In addition, from Equation 11, we can see that the amplitude of the ocean wave force on the harvester increases with an increment of the wave height which results in a rise of power output as seen by Equation 24. It is known that the ocean having at wave heights greater than 2 m dominates a very small area of the world ocean.

Figure 8 shows the effect of the number of rotator blade, m, on the RMS of the generated power with various wave period, $T = 7$ and 13 seconds and other parameters $n_l = 15$, $d_m = 0.25$ m, $H_w = 1.5$ m, $d = 0.002$ m, and $Wo = 1$ m. It is illustrated in the figure that the generated power increases nonlinearly with an increase in the rotator blade number. A RMS of 210 W can be realized at the rotator blade number, $m = 18$, and wave period, $T = 7$ sseconds. It is interpreted that, based on Equation 18, the excitation frequency of the magnetic force is directly propositional to the blade number; hence,

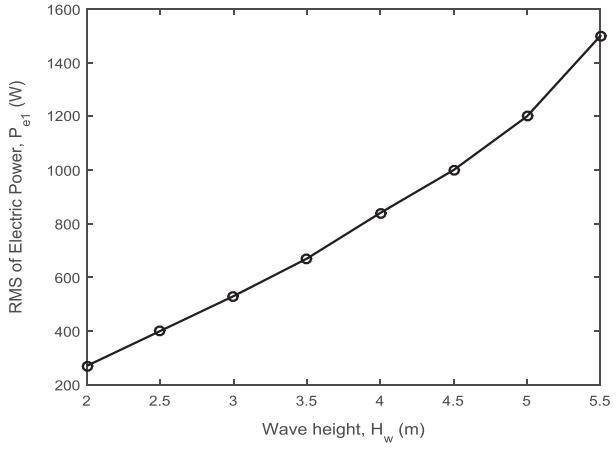

FIGURE 7 Variation of power RMS with respect to the wave height

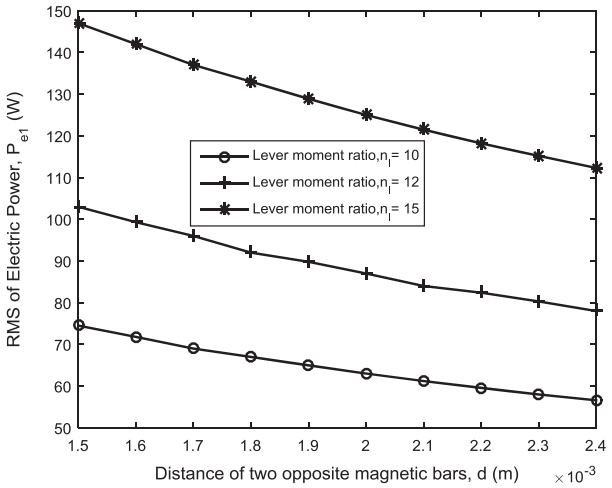

FIGURE 9 Effect of the distance between 2 opposite magnetic bars on RMS of the power with different lever moment ratios

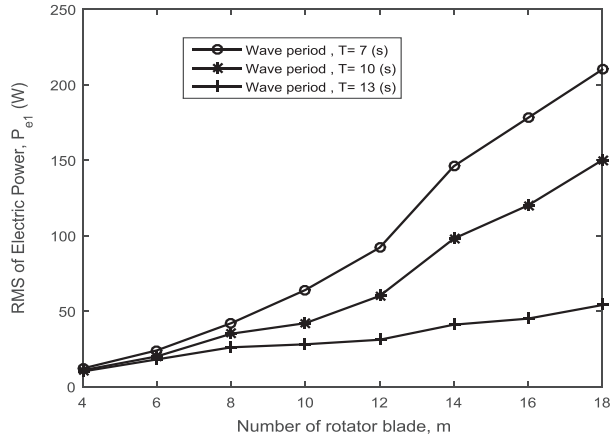

FIGURE 8 Effect of the number of rotator blade on RMS of the power with different wave period

increasing the blade number results in a rise in generated power. The figure also reveals that RMS increases with a decrease in the wave period. That is due to the fact that, as described in Equation 17, the angular frequency of rotator is inversely proportional to the wave period. Hence, an increase in the wave period leads to a lower excitation frequency. From this observation, we can conclude that the ocean region with a long wave period degrades the energy conversion capability of conventional harvesters. Nevertheless, the figure exhibits an interesting and useful finding that the proposed harvester can improve its power output by increasing the blade number, when it operates on the ocean floor with a long wave period.

Figure 9 shows the effect of the distance between 2 opposite magnetic bars on the RMS of the power output with various lever moment ratios at $d_m = 0.25$ m, $H_w = 1.5$ m, $T = 7$ seconds, $m = 15$, $Wo = 1$ m. The figure indicates that the RMS of 1 generator is up to 148 W at a distance of $d = 1.5$ mm and lever moment ratio of $n_l = 15$. The figure reveals a nonlinear reduction of power output, when the distance of 2 opposite magnetic bars increases. The observed phenomenon can be explained that increasing the separation between 2 opposite magnetic faces leads to a lower magnetic flux density, which in turn results in a lower repelling force. The value of gap d ranging from 1 to 2 mm is frequently used in applications.[15,16,35,36] The figure also indicates that RMS of generated power increases with a rise in the lever moment ratio. The reason lies in the fact that, through the lever mechanism, the force magnitude acting on the piezoelectric transducer at the tip point, A, of lever is magnified n_l times with respect to the force magnitude at the tip point, C. It concludes that the lever also plays an important role in the harvester to improve the power output.

From the modeling, we see that it is important to understand the energy conversion efficiency of proposed harvester and the effect of the harvester width on the efficiency. Figure 10 shows the effect of the harvester width on its energy conversion efficiency based on Equation 34 with parameters used as $d = 0.002$ m, $d_m = 0.25$ m, $H_w = 1.5$ m, $T = 7$ seconds, $m = 15$, $n_l = 15$. From the figure, harvester conversion efficiency is around 1% at a harvester width being 1 m. It is demonstrated by Figure 10 that an increment in the harvester width leads to a slight reduction of the conversion efficiency. It may be interpreted that a larger harvester will have the higher viscous and radiation damping forces created by the wave-harvester interaction. These damping dissipates the ocean wave energy subjected to the harvester ballast, before the ocean wave energy is converted into the electric power by the internal components of harvester.

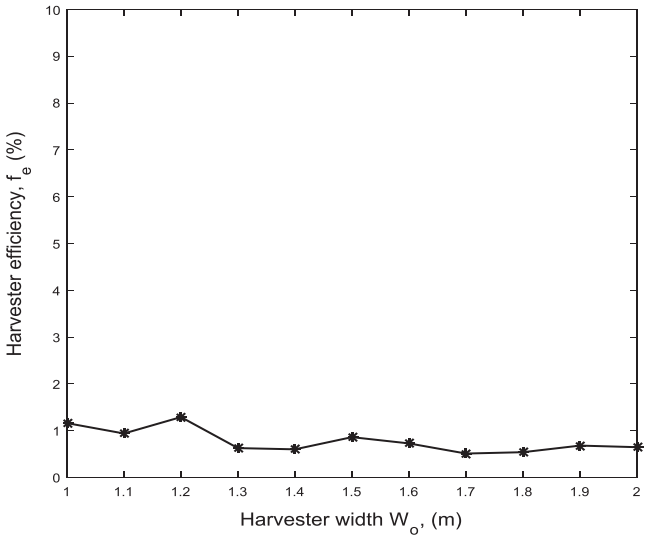

FIGURE 10 The energy conversion efficiency of the harvester with respect to different harvester width

Table 3 shows a comparison between the proposed harvester and the snake-like structure "Pelamis"[37] in terms of total generated power at the same weight. The data used for the comparison are selected as $d = 0.002$ m, $d_m = 0.3$ m, $H_w = 1.5$ m, $T = 7$ seconds, $m = 15$, $n_l = 15$. It is noted in Table 3, the total weight of the proposed harvester units is set equal to the weight of a Pelamis. The weight of a unit is estimated by a sum of weight of individual components, which are referred to their material dimensions and properties. Table 3 shows that the total power output of harvester units is 7020 kW, which is approximately 9 times higher than that of a Pelamis. In addition, the internal components of harvester are simpler and more eco-friendly than Pelamis, which is made of complex fluid pipes, electronic components, and hydraulic piston-cylinders. As a result, for a long-time operation, the developed harvester exhibits a better benefit than Pelamis, and the maintenance of the proposed harvester is easier than the Pelamis. Furthermore, the proposed harvester contains mainly the mechanical components and less gear lubrication fluid. There is, therefore, no concern of contaminating the marine environment by presence of the proposed harvester.

TABLE 3 Comparison between proposed harvester and snake-like structure, Pelamis

	Proposed harvester	Pelamis
Total weight (kg)	1 350 000	1 350 000
Weight of unit (kg)	100	337 500
Number of unit	13 500	1
Total power output (kW)	7020	750

4 | CONCLUSION

A novel harvester is developed to harness the energy from ocean waves. The internal structure of the harvester consists of rack and pinion actuator connecting with 2 generators. The generator has a rotator having magnetic bars attached on its blade tip and a stator comprised of mass, spring, lever, and piezoelectric transducer. In summary, the findings of the present research are as follows:

- The harvester produces a converted frequency of mechanical vibrator 30 times higher than that of ocean wave source.
- The RMS of power output increases with increases in the ocean wave height, lever moment ratio, number of magnetic bar in the rotator and with decreases in the wave period, the distance between 2 opposite magnetic bars, and submerged part height.
- For the proposed harvester with geometric parameters of $H_o = 1$ m, $L_o = 1$ m, $W_o = 1$ m and submerged part height being $d_m = 0.3$ m, RMS of 1 generator is up to 260 W at ocean wave height and period being $H_w = 2$ m, and $T = 7$ seconds, respectively.
- Total generated power of harvesters is 9 times higher than that produced by Pelamis, when both harvesters are at the same weight.

The proposed harvester is environmentally friendly and can be a promising candidate for efficiently generating electricity used in the marine and civil applications.

REFERENCES

1. Energy information agency (EIA). [Internet] [Cited 2016 May 15th]. Available from http://www.eia.gov/tools/faqs/faq.cfm?id=77&t=11.
2. Falnes J. A review of wave-energy extraction. *Mar Struct*. 2007;20:185-201.
3. Zhang YL, Lin Z. Advances in technology of ocean wave energy converters using piezoelectric materials. *J Hydraul Eng*. 2011;5:324-331.
4. Anton SR, Sodano HA. A review of power harvesting using piezoelectric materials 2003–2006. *Smart Mater Struct*. 2007;16:21-27.
5. Ocean Power Technologies Case Study. [Internet] [Cited 2016 Jun 15th]. Available from http://acore.org/wp-content/uploads/2012/01.
6. Sravanthi C, James MC. A survey of energy harvesting sources for embedded systems. 2008 IEEE.
7. Williams CB, Yates RB. Analysis of a micro-electric generator for microsystems. *Sensors Actuators A*. 1996;52:8-11.

8. Priya S. Advances in energy harvesting using low profile piezoelectric transducers. *J Electroceram*. 2007;19:165-182.
9. Piezoelectric system. [Internet] [Cited 2016 December 15th]. Available from http://www.piezo.com/tech3faq.html.
10. Gu L, Livermore C. Passive self-tuning energy harvester for extracting energy from rotational motion. *Appl Phys Lett*. 2016;97:04-09.
11. Murray R, Rastegar J. Novel two-stage piezoelectric-based ocean wave energy harvesters for moored or unmoored buoys. Act and Pas Smart Structure and Integrated Systems. *Proc SPIE*. 2009;7288:1117-1129.
12. Miller LM, Wright PK, Ho CC, Evans JW, Shafer PC, Ramesh R. Integration of a low frequency, tunable MEMS piezoelectric energy harvester and a thick film micro capacitor as a power supply system for wireless sensor nodes in IEEE, ECCE; 2009:27–34.
13. Zhou S, Cao J, Erturk A, Lin J. Enhanced broadband piezoelectric energy harvesting using rotatable magnets. *Appl Phys Lett*. 2013;102:01-05.
14. Erturk A, Hoffmann J, Inman DJ. A piezomagnetoelastic structure for broadband vibration energy harvesting. *Appl Phys Lett*. 2009;94:02-06.
15. Zhou S, Cao J, Inman DJ, Liu S, Wang W, Lin J. Impact-induced high-energy orbits of nonlinear energy harvesters. *Appl Phys Lett*. 2015;106:01-06.
16. Xie XD, Wang Q, Wu N. A ring piezoelectric energy harvester excited by magnetic forces. *Int J Eng Sci*. 2014;77:71-78.
17. Shu X Piezoelectric thin films and nanowires: synthesis and characterization. Master thesis, Georgia Institute of Technology, 2011.
18. McCormick M. *Ocean Engineering Mechanics with Applications*. New York: Cambridge University Press; 2009.
19. McCormick M. *Ocean Wave Energy Conversion*. Mineola, NY: Dover Publications; 2007.
20. Rafael EV, Carl DC, Julio CC. Analysis of a planar tensegrity mechanism for ocean wave energy harvesting. *J Mech Robot*. 2014;6:31015-31021.
21. Kristiansen E, Egeland O. Frequency dependent added mass in models for controller design for wave motion ship damping. 6th IFAC Conference on Manoeuvring and Control of Marine Craft (MCMC'03), Girona, Spain, September 2003:17–19.
22. Taghipour R, Perez T, Moan T. Hybrid frequency–time domain models for dynamic response analysis of marine structures. *Ocean Eng*. 2008;35(7):685-705.
23. Vasquez RE. Analysis of a tensegrity system for ocean wave energy harvesting. Ph.D. thesis, Gainesville, FL: University of Florida; 2011.
24. Drag Coefficient. [Internet] [Cited 2016 August 25th]. Available from https://en.wikipedia.org/wiki/Drag_coefficient.
25. K&J Magnetics. The original K&J magnet calculator. 2011. [Internet] [Cited 2016 May 15th]. Available from www.kjmagnetics.com/calculator.asp.
26. Neodymium. [Internet] [Cited 2016 August 15th]. Available from http://www.intemag.com/magnetic_properties.html#neodymium_props.
27. Al-Ashtari W, Hunstig M, Hemsel T, Sextro W. Frequency tuning of piezoelectric energy harvesters by magnetic force. *Smart Mater Struct*. 2012;21:19-24.
28. Viet NV, Xie XD, Liew KM, Banthia N, Wang Q. Energy harvesting from ocean waves by a floating energy harvester. *Energy*. 2016;112:1219-1226.
29. Blevins RD. *Formulas for Natural Frequency and Mode Shape*. New York: Van Nostrand Reinhold; 1979.
30. Woodhouse J. Linear damping models for structural vibration. *J Sound Vib*. 1998;215(3):547-569.
31. Mitcheson PD, Yeatman EM, Rao GK, Holmes AS, Green TC Energy harvesting from human and machine motion for wireless electronic devices. *Proc IEEE* 96: 1455–1458.
32. Xie XD, Wang Q. Energy harvesting from a vehicle suspension system. *Energy*. 2015;86:385-392.
33. Ravi TT, Krishna CT. Computation of natural frequencies of multi degree of freedom system. *Int J Eng Res Technol*. 2012;10:2278-2281.
34. Wu N, Wang Q, Xie XD. Wind energy harvesting with a piezoelectric harvester. *Smart Mater Struct*. 2013;22:23-28.
35. Jiang H, Kiziroglou ME, Yates DC, Yeatman EM. A motion-powered piezoelectric pulse generator for wireless sensing via FM transmission. *IEEE Internet Things J*. 2015;2:5-10.
36. Su WJ, Zu J. An innovative tri-directional broadband piezoelectric energy harvester. *Appl Phys Lett*. 2013;103:22-27.
37. Pelamis Wave Energy Converter. [Internet] [Cited 2016 May 15th]. Available from https://en.wikipedia.org/wiki.

How to cite this article: Viet NV, Wang Q, Carpinteri A. Development of an ocean wave energy harvester with a built-in frequency conversion function. *Int J Energy Res*. 2018;42:684–695. https://doi.org/10.1002/er.3851